Combining high hardness and crack resistance in mixed network glasses through high-temperature densification

Saurabh Kapoor, Kacper Januchta, Randall E. Youngman, Xiaoju Guo, John C. Mauro,

Mathieu Bauchy, Sylwester J. Rzoska, Michal Bockowski, Lars R. Jensen, and Morten M.

Smedskjaer

Combining high hardness and crack resistance in mixed network glasses through high temperature densification

Saurabh Kapoor[1], Kacper Januchta[1], Randall E. Youngman[2], Xiaoju Guo[2], John C. Mauro[3], Mathieu Bauchy[4], Sylwester J. Rzoska[5], Michal Bockowski[5], Lars R. Jensen[6], Morten M. Smedskjaer[1,*]

[1]*Department of Chemistry and Bioscience, Aalborg University, Aalborg, Denmark*
[2]*Science and Technology Division, Corning Incorporated, Corning, USA*
[3]*Department of Materials Science and Engineering, The Pennsylvania State University, University Park, USA*
[4]*Department of Civil and Environmental Engineering, University of California, Los Angeles, USA*
[5]*Institute of High-Pressure Physics, Polish Academy of Sciences, Warsaw, Poland*
[6]*Department of Materials and Production, Aalborg University, Aalborg, Denmark*
*Corresponding author. e-mail: mos@bio.aau.dk

ABSTRACT

Obtaining a combination of high toughness and strength is crucial for most structural materials, but unfortunately these tend to be mutually exclusive. The search for strong and tough damage-resistant materials has thus typically been based on achieving an acceptable compromise between hardness and crack resistance. Focusing here on brittle oxide glasses, we propose a new strategy for overcoming this conflict by identifying new structural motifs for designing hard and crack-resistant glasses. Specifically, we report that surprisingly there is no decrease in the densification contribution to deformation of a mixed network Al_2O_3-B_2O_3-P_2O_5-SiO_2 bulk glass following pre-densification of the glass at elevated temperature. Hitherto unique to this glass composition, the treatment reduces the residual stress during subsequent sharp contact loading, which in turn leads to a simultaneous increase in hardness and crack resistance. Based on structural characterization, we show that the more densified medium-range order of the hot compressed glass results in formation of certain structural states (e.g., non-ring B^{III}), which could not be reached through any composition or thermal path. This work thus shows that accessing such "forbidden" structural states through the identified densification at elevated temperatures offers a way forward to overcome the conflict of strength versus toughness in structural materials.

I. INTRODUCTION

All structural materials for engineering applications should ideally feature a combination of high strength, hardness, toughness, and damage resistance, but unfortunately some of these tend to be mutually exclusive in many materials. That is, when a material is able to undergo plastic deformation easily, the local high stresses can be dissipated, thus avoiding fracture or vice versa [1]. The mechanism of such inelastic deformation is highly material-dependent. Dislocation motion is well-known for crystalline solids, but other mechanisms have been reported, including sliding in tooth dentine and bone [2], phase transformations in metals and ceramics [3], frictional motion in seashells [4], and shear band propagation in glassy metals [5]. Twinning-induced plasticity in metals can also be used to impede dislocation motion and induce strengthening and ductility [5], whereas it is believed that brittle oxide ceramics and glasses cannot be toughened by promoting inelastic deformation [7]. Alternative toughening mechanisms for oxide glasses include crack deflection due to local heterogeneity [1].

Functional and transparent oxide glasses with tailored properties are expected to play a critical role in a range of developing technologies [8], but their brittleness and low practical strength are major bottlenecks for future applications. Any impact or scratch events leading to formation of cracks amplify local tensile stresses, resulting in catastrophic failures. Therefore, increasing the hardness and crack resistance of glasses is critical for the development of scratch-resistant and mechanically durable glasses [9]. The resistance to elastoplastic deformation, known as hardness, has been found to correlate positively with the connectivity and atomic packing density in oxide glasses, i.e., more compact and connected glasses exhibit higher hardness [10-16]. Approaches such as compositional variation and thermal treatments have traditionally been employed to design harder glasses through an increasing atomic packing density [9, 17-21]. Al_2O_3–R_2O_3 and Al_2O_3–SiO_2–R_2O_3 glasses (R: Y, Sc, or Ta) are among the hardest oxide glasses (Vickers hardness approaching ~10 GPa) [10, 22-24]. However, designing glasses with improved hardness through structural tuning, typically also results in lower resistance to crack initiation and growth [21, 25]. Though nitridation [26] and chemical strengthening [27] are notable exceptions, the former typically results in non-transparent bulk glasses [28] and the latter is an expensive

2

and time-consuming post-processing technique. As such, there remains an interest in developing new approaches to overcome the conflict between hardness and damage resistance in this class of materials. Therefore, identification of intrinsic structural motifs that improve both hardness and crack resistance are critical for the development of new scratch-resistant and mechanically durable glasses.

As a method for modifying the glass structure and properties, pressure densification of glasses at temperatures around the glass transition temperature T_g (so-called hot compression) has attracted recent [29]. Application of pressure at high temperature expands the region of phase space accessible to the glass, i.e., it enables access to so-called "forbidden structural states" that are inaccessible through compositional and thermal variation alone [30]. Considerable studies have been performed to elucidate the effects of composition and thermal history on the mechanical properties of glasses [31-33], but pressure can be used as an additional degree of freedom or design parameter to tailor and understand the glass structure-property relations [29]. In addition, high-pressure densification has also played a pivotal role in understanding the deformation and fracture behavior of glasses [29]. Glasses tend to accommodate high stress levels via a complex interplay of elastic deformation, densification, and shear flow, which in turn involves local structural rearrangements [34]. Densification through thermal and/or pressure history variation has been shown for numerous glass compositions to result in harder but less crack-resistant glasses [25]. However, in this paper, we report the evidence of an unusual and unexpected exception to this "rule" for a mixed network-former glass, where densification leads to both higher hardness and crack resistance. This is achieved by accessing a forbidden structural state through a high temperature densification treatment.

The object of this study is a modifier-free mixed network glass with molar composition $4Al_2O_3$-$28B_2O_3$-$10P_2O_5$-$58SiO_2$. Such mixed network-former glasses are candidate materials for consumer electronic devices, e.g., due to their low thermal expansion coefficient [35]. We show that the simultaneous increase in hardness and crack resistance of this glass upon hot compression arises from an increase in the contribution from densification to indentation deformation following hot compression, i.e., the decrease in free volume of the glass unexpectedly facilitates further densification. Based on work over

3

the last decade, higher free volume in glasses is expected to yield higher crack resistance due to the larger densification contribution during sharp contact loading [21]. We also perform standard sub-T_g annealing treatment that, as expected, results in a denser, harder but less-crack resistant glass. Using structural characterization techniques, we show that densifying the glass at high temperature facilitates the formation of certain structural states, which are inaccessible through traditional methods of structural modification. The accessed forbidden state appears to increase the local flexibility of the glass network despite the overall compaction, in turn facilitating further densification during indentation. This study thus shows for the first time that densification under sharp contact loading is not significantly affected by hot compression. This is achievable by careful tuning of structural parameters irrespective of the decrease in free volume upon compression.

II. EXPERIMENTAL SECTION

A. Sample preparation

The Al_2O_3-B_2O_3-P_2O_5-SiO_2 glass was synthesized using traditional melt-quenching technique, with reagent grade silica, calcined alumina, boric acid, and boron orthophosphate as raw materials. Appropriate quantities of these powders were mixed and melted in a silica crucible at 1650 °C for 5 hours and then roller quenched. To improve the chemical homogeneity, the glass was re-melted in a silica crucible at 1650 °C for 5 hours and casted onto a stainless steel plate. The chemical composition of the final glass was determined using inductively coupled plasma optical emission spectroscopy and found to be $3.9Al_2O_3$-$27.7B_2O_3$-$10.0P_2O_5$-$58.4SiO_2$ (in mol%, ±0.1). The glass was annealed for 30 min at its glass transition temperature (T_g), which was found to be 768 K using beam bending viscometry. Powdered glass samples were used for x-ray diffraction measurements (Empyrean XRD, PANalytical), showing no signs of crystallization before or after hot compression (spectra not shown).

Glass samples with dimensions of about $12 \times 12 \times 3$ mm^3 were cut and the flats were ground and polished in water using SiC adhesive discs with increasing grit size. The final steps of polishing were carried out in a water-free diamond suspension on a polishing cloth in order to prevent surface hydration.

These specimens were subjected to an isostatic N_2-mediated pressure treatment at 1 GPa. The compression was carried out by maintaining the given value of pressure at T_g for 30 min, and subsequently quenching with an initial cooling rate of 60 K/min. The pressure chamber was then decompressed at a rate of 30 MPa/min. This treatment method is described in more detail in Ref [29].

B. Mechanical characterization

Density values of the glass specimens were determined using Archimedes' principle of buoyancy. The weight of each specimen (at least 0.30 g) was measured in air and ethanol ten times. Vickers micro-indentation (Duramin 5, Struers) measurements were performed to determine hardness and crack resistance. 30 symmetrical indents were produced at 8 different loads (245 mN to 19.6 N) with a loading time of 15 s. The indents were evaluated after each indentation using optical microscopy. The indent diagonal length as well as the number of the radial/median cracks emanating from the indent corners were recorded.

Following the method described in Ref. [13], the extents of indentation-induced densification and shear flow were quantified for the investigated glass samples. The topographical images of 10 indents produced at 245 mN were acquired using atomic force microscopy (AFM, Ntegra, NT-MDT) before and after a thermal annealing at $0.9T_g$ (691 K) for 2 h. Silicon tip cantilevers (VIT_P, NT-MDT) were used in semi-contact mode with a scanning frequency of 0.5 Hz to create 16 x 16 μm^2 images with a resolution of 256 x 256 pixels. The acquired images were analyzed with a custom-written MATLAB script to quantify the volume recovery ratio.

Room temperature ultrasonic measurements were performed using the pulse-echo method with an ultrasonic thickness gauge (38DL Plus, Olympus). The longitudinal and shear wave velocities (V_L and V_S, respectively) were determined from the specimen thickness (3–6 mm) of two parallel faces (polished with 1 μm diamond suspension) and the delay time Δt_L and Δt_S between successive signals. From the ultrasonic velocities and density, the elastic constants were calculated [36].

C. Structural characterization

Raman spectroscopy measurements were conducted at room temperature to obtain structural information at short- and intermediate-range length scales. This was done using a Renishaw in Via micro-Raman spectrometer with 532 nm laser in the range from 200 to 1600 cm^{-1}. The measurements were performed on as-prepared and compressed samples. Furthermore, for the as-prepared and compressed glass, the micro-Raman spectrometer was utilized in the mapping mode to acquire spectra at different positions around a Vickers indent produced at 1 kgf. The laser beam was focused on the center of the indent, and spectra were collected at interval of 20 µm at 5 different locations away from the center towards the edge and outside of the indent. All of the recorded spectra were subjected to a baseline correction and normalization procedure.

Solid state nuclear magnetic resonance (NMR) spectra of ^{31}P and ^{11}B were obtained using a commercial spectrometer (Agilent DD2) in conjunction with an 11.7 T superconducting magnet. The resonance frequencies of ^{31}P and ^{11}B at this external field strength are 202.30 and 160.34 MHz, respectively. All of the glasses were powdered immediately before analysis, and packed in 3.2 mm zirconia rotors for sample spinning at 20 kHz. ^{31}P magic angle spinning (MAS) NMR spectra were acquired with a $\pi/6$ pulse width, a delay time of 60 s and as a composite of ~1500 free induction decays. ^{11}B MAS NMR spectra were acquired with a $\pi/12$ pulse width of 0.6 µs, a delay time of 10 s and as a composite of ~1000 free induction decays. MAS NMR data were processed with minimal apodization and shift referenced to 85% phosphoric acid at 0.0 ppm for ^{31}P and aqueous boric acid at 19.6 ppm for ^{11}B.

^{11}B triple quantum magic angle spinning (3QMAS) NMR experiments were conducted at 11.7 T (160.34 MHz resonance frequency) using a 3.2 mm MAS NMR probe and sample spinning of 20 kHz. The hard $3\pi/2$ and $\pi/2$ pulse widths were optimized to 2.6 and 1 µs, respectively. Data were collected using the three pulse, zero quantum filtering method, with a z-filter delay of 10 µs and a soft reading pulse of 20 µs [37]. 120 scans were collected for each of 256 t_1 points, incorporating a recycle delay of 1s.

Spectra were processed using commercial software (VNMJ, Agilent), without any additional apodization in either time domain, and referenced to aqueous boric acid at 19.6 ppm.

^{27}Al MAS and 3QMAS NMR experiments on both as-prepared and compressed (1.0 GPa) glass were conducted at 16.4 T using a commercial spectrometer (VNMRs, Agilent) and a 3.2 mm MAS NMR probe (Agilent) with spinning speeds of 20 kHz. MAS NMR data were acquired using radio frequency pulses of 0.6 μs (equivalent to a $\pi/12$ tip angle), relaxation delays of 2 s, and signal averaging of 2000 acquisitions. MAS NMR data were processed using commercial software, without additional apodization, and referenced to aqueous aluminum nitrate at 0.0 ppm. ^{27}Al 3QMAS NMR spectra were measured using the three pulse, zero quantum filtering method [37]. The hard $3\pi/2$ and $\pi/2$ pulse widths were calibrated to 2.8 and 1 μs, and the soft reading pulse of the z-filter was optimized to 15 μs. 120 to 240 scans were collected for each of 64 to 88 t_1 points, using a recycle delay of 1 or 2 s. Spectra were processed using commercial software (VNMRJ, Agilent), and modest line broadening (50 Hz) was used in processing the ^{27}Al 3QMAS NMR data.

^{11}B and ^{27}Al MAS NMR spectra were deconvoluted using DMFit,[38] which provides proper 2nd-order quadrupolar lineshapes for B^{III} resonances, and with the "simple Czjzek" model, a means by which to adequately fit ^{27}Al MAS NMR spectra of glasses [39].

III. RESULTS

A. Mechanical properties

Compression at 1 GPa of the mixed network glass at its T_g (768 K) results in changes in its structure and intrinsic free volume, which in turn leads to a permanent increase in density from 2.167 to 2.229 g/cm^3, in qualitative agreement with the previous studies on other oxide glasses [40-43]. Shannon radii of atoms are used to calculate the atomic packing density (C_g), which is the ratio between the theoretical volume of ions (assumed to be spherical) and the actual molar volume of the glass [44]. We find an increase in C_g from 0.39 to 0.47 upon compression (Table S1 in the Supplemental Material [45]). We also find the usual

pressure-induced increase in Vickers hardness (H_V) (Fig. 1) [42]. Previous studies have suggested that the overall network densification is responsible for the increase in hardness upon compression [16, 29, 42, 46, 47]. Furthermore, density and hardness also increase upon annealing of the glass at $0.9T_g$ (691 K) at ambient pressure due to the decrease in fictive temperature, in agreement with earlier findings [25].

Elastic moduli of glasses generally depend on the packing density and interatomic bond energies [48]. In agreement with previous findings [49], all of the elastic moduli of the glass increase upon densification via both annealing and hot compression (Figure 1 and Figure S1 in the Supplemental Material [45]), while the Poisson's ratio (v) remains almost constant post densification (Table S1 in the Supplemental Material [45]). This significant stiffening resulting from densification by annealing and compression is primarily attributed to the increased packing efficiency of the glass. Furthermore, we note that the pressure-induced increase in H_V is more pronounced than that in elastic moduli, resulting in a general decrease in the elastoplastic ratio E/H (Table S2 in the Supplemental Material [45]). This corresponds to an increase in the elastic recovery upon indenter unloading [50] and a decrease in the fracture process zone, which relates to the typical size of the region in front of the crack tip [51].

To evaluate the cracking behavior of the samples, we calculated the crack resistance (CR), which is defined as the load where the probability for radial/median cracking is 50%, i.e., an average of two cracks emanating from the four corners of each indent [13, 43, 52]. CR is determined by counting the number of radial/median cracks at systematically increasing indentation load, resulting in an error within ±0.1 kgf. As expected [25], CR of the investigated glass (0.95 kgf) decreases upon sub-T_g annealing (0.25 kgf). Surprisingly, an increase in CR from 0.95 kgf to 1.45 kgf is observed upon hot compression (Fig. 2a). All the previous studies on various oxide glass families have reported a pronounced increase in the crack initiation probability with increasing degree of densification (Fig. 2b) [11-13, 46], which has been ascribed to the reduced capability of the hot compressed glass to accommodate stress via further densification during indentation [13]. Here, hot compression enhances the ability of the mixed network glass to accommodate the applied mechanical stress, as seen from the indent images produced at 1 kgf in Fig. 2c.

Most of the existing literature on the mechanical behavior of glasses suggests that *CR* is correlated with the intrinsic free-volume in the glass structure, facilitating densification under stress, which in turn dissipates the stresses accumulated during indentation [21, 53]. Reducing the residual stress is considered as one of the primary mechanisms for inhibiting crack formation. We have therefore studied the indentation deformation mechanism of the present glass by quantifying the contributions of shear flow and densification volume to the total indentation deformation volume. This is done by annealing the indented glass at $0.9T_g$, which is sufficient to activate local structural rearrangements and thus recover the indentation-induced densification of the glassy network. On the other hand, the viscosity is too high for any significant viscous flow during the timescale of the annealing (2 h) [21, 53]. By combining this annealing approach with AFM measurements of the indent topography, we can decouple and quantify the two indentation deformation mechanisms (Fig. 2d). The ratio between these two volume-displacement mechanisms is defined as the volume recovery ratio (V_R). Previous studies have positively correlated V_R to *CR* [21, 53, 54]. In the present investigation, the observed value of V_R changes from 0.75±0.03 for the as-prepared sample to 0.73±0.04 for the sample, which has been pre-densified through prolonged sub-T_g annealing at ambient pressure, in agreement with expectations [25]. However, we observe an unusual change in V_R from 0.75±0.03 to 0.79±0.05 upon hot compression (Table S1 in the Supplemental Material [45]), arising from an apparent increase in the extent of densification during indentation. This unusual change in V_R is attributed to the enhanced ability of the network-forming cations to change their local chemical environment upon indentation, facilitating compaction and resulting in lower residual stress and thus diminished driving force for cracking [52]. Finally, we note that although the apparent increase in V_R upon compression is very small (and within the error range), the main finding is that the result is in sharp contrast to the previously studied alkali aluminosilicate glasses. The latter exhibit a significant *decrease* in V_R from ~0.80 to 0.65 upon hot compression [13].

B. Structural basis for increase in densification and crack resistance

To understand the structural origin of the pressure-induced increase in crack resistance of the present mixed network glass, we compare the short- and medium-range order changes induced by both indentation and hot compression using Raman spectroscopy. The spectra of the as-prepared and hot compressed glasses are shown in Figure 3. In the low-frequency region from 200 to 700 cm^{-1}, a strong band centered near 460 cm^{-1} is observed, which can be jointly attributed to both Si-O-Si and Si-O-Al vibrations [55]. The differentiation of their individual contributions to the band is challenging because the signal of Q^n (n represents the number of bridging oxygen per tetrahedron) species mixes both SiO_4 and AlO_4 contributions [55]. Moreover, this region exhibits a long tail towards the low frequency around ~200 cm^{-1}, which has been attributed to the stretching of oxygen atoms in five-, six- or higher-membered rings [55]. Compression results in decrease of the bandwidth, interpreted as a decrease in distribution of bond angles [56, 57], i.e., a more organized local structure around Si and Al in the compressed glass. In addition, this band shifts towards higher frequency upon compression suggests a decrease in Si-O-Si and Si-O-Al bond angles [56]. The mid-frequency region (700–900 cm^{-1}) shows evidence of a band representing boroxol rings present around ~805 cm^{-1}, arising due to symmetric breathing motion of the oxygens within the ring, thus not influenced by the oxygen motion associated with Si, Al or P atoms [58]. The investigated glass also exhibits a band at ~930 cm^{-1}, indicative of formation of B-O-P linkages. The other very weak band observed near 730 cm^{-1} can be assigned to the B−O stretching vibration associated with four-fold coordinated boron linked to other borate species [59].

Hot compression decreases the intensity of the ~805 cm^{-1} band (Fig. 3). Since there is no formation of new bands related to four-fold coordinated boron, this decrease is due to pressure-induced ring breakage [60], i.e., a structural change in the medium-range order. A conversion of boroxol rings into non-rings has previously been found to accompany densification of glassy B_2O_3 at both elevated temperature [29] and room temperature [61]. Furthermore, the absence of narrow Raman bands around 770 cm^{-1} indicates that the BO_4 units present in the glass are not in the form of well-defined rings (e.g., triborate or other super-structural units), but rather associated with BPO_4 units, in agreement with the NMR results discussed below. The high frequency region (900–1300 cm^{-1}) consists of a broad envelope

centered around 1150 cm^{-1}, which is attributed to $AlPO_4$ and BPO_4 vibrations, as crystalline $AlPO_4$ and

BPO_4 have Raman active bands in the region from 1120 and 1170 cm^{-1}, respectively [62-64]. The weak

band around 1315 cm^{-1} is likely due to stretching vibrations of O=P double bond. The width of this band

decreases slightly upon hot compression (Fig. 3), indicating a decrease in the bond angle distribution of

PO_4 tetrahedra upon hot compression.

Micro-Raman spectra have also been acquired on the indent imprint (produced at 1 kgf) of the as-

prepared (Fig. 4a) and hot-compressed (Fig. 4b) samples to compare their indentation-induced structural

changes. Indentation of the as-prepared glass results in a new sharp peak around 500 cm^{-1}, which is

attributed to D_1 band corresponding to four-membered SiO_4 rings [65]. Similar changes have been

observed upon indentation of SiO_2 glass [66]. Indentation also causes the broad band at 460 cm^{-1} to shift

towards 495 cm^{-1} with a simultaneous decrease in the full width at half maximum (FWHM). As shown by

Furukawa *et al*. [67], the frequency of the stretching/bending modes of Si-O-Si bridges increases upon

decrease of the Si-O-Si angle. The distribution of Si-O-Si bond angles thus becomes narrower and shifts

to smaller values upon indentation, manifesting the structural rearrangements leading to the densification

of the silicate sub-network. It is noteworthy that indentation of the hot compressed glass is not

accompanied by appearance of D_1 or D_2 bands which are assigned to four- and three-membered SiO_4

rings, respectively [65] (Fig. 4b). Furthermore, relatively smaller peak shifts are observed upon

densification at elevated temperature compared to indentation-induced densification. Similar to hot

compression (Fig. 3), indentation results in decreasing peak intensity of boroxol rings in both as-prepared

and compressed glasses. In addition, indentation also decreases the FWHM of the peak in the high

frequency region (Fig. 4), which could be due to the distortion of BPO_4 and $AlPO_4$ units. However,

indentation of the as-prepared glass leads to a new strong peak around 880 cm^{-1} (Fig. 4a), which

corresponds to pyroborates in glasses containing multiple network formers [68]. Such formation is not

observed in hot compressed glass and has not been observed in previous studies on densified borate

glasses [66, 69]. The band is not present in Raman spectra of the as-prepared glass obtained at lower

indentation loads (<1 kgf), where there is also no crack formation. As such, we propose the band is

related to destruction of interconnected network units due to breakage of larger units, resulting in smaller, highly charged groups like pyroborates [70]. Additional work is needed to clarify the charge compensation mechanism for such charged pyroborate units.

In the following, we employ solid state NMR spectroscopy to further identify the structural features which enable the hot compressed glass to accommodate mechanical stress more favorably than the as-prepared glass. Fig. 5a shows the ^{11}B MAS NMR spectra, with the deconvolution results summarized in Table 1. In both glasses, the network consists of trigonal and tetrahedral boron, as shown by the broad resonance between 0 and 20 ppm and the much narrower feature centered around -4 ppm, respectively. The ^{11}B MAS NMR data were fit using DMFit to reproduce B^{III} and B^{IV} line shapes, and for both spectral regions, and for both glasses, two distinct peaks were required to adequately reproduce the experimental data. The trigonal boron resonance is comprised of both ring (~18 ppm) and non-ring (~13 ppm) components [71], with most of the trigonal boron assigned to non-ring sites (B^{III} non-ring) in the as-prepared and compressed glass. Further evidence for both types of trigonal boron sites can be seen in the ^{11}B 3QMAS NMR data (Figure S2 in the Supplemental Material [45]), where the contour plots for the as made and compressed glasses both exhibit multiple features in the frequency region attributed to trigonal boron. Since the excitation and detection of 3QMAS NMR signal is comparable for both trigonal sites, due to very similar magnitudes of their quadrupolar coupling constants (Table 1), the isotropic projections from ^{11}B 3QMAS NMR spectra can also be evaluated for relative concentrations of these trigonal sites. Figure 5b shows the isotropic projection for the trigonal boron peaks, where the spectra for both glasses have been fit using two Gaussian peaks. These isotropic projections clearly show the presence of two types of trigonal boron (ring and non-ring), and their relative intensities are consistent with the MAS NMR results in Table 1. The tetrahedral boron (B^{IV}) peak centered around -4.1 ppm shows an asymmetric shoulder around -2 ppm, indicating the formation of two types of B^{IV} environments. The former is due to B^{IV} units with only P as next nearest neighbor (NNN), i.e., BPO_4-like units [72], while the latter minor peak is most likely due to B^{IV} units with partial replacement of P NNN with Si. The chemical shift of this

second B^{IV} site is likely too shielded to be assigned to tetrahedra without any P NNN, as even B^{IV} surrounded entirely by Si NNN has a chemical shift of around -1.4 ppm [73].

Among the network forming cations in the investigated glass, boron undergoes the largest pressure-induced changes. That is, the ratio of relative fraction of B^{III} ring to B^{III} non-ring units decreases from 0.25 to 0.15 upon hot compression (Table 1), along with a minor change in the B^{IV} fraction (from 20.6 to 20.4 at%), as shown in Figure S3 in the Supplemental Material [45]. The spectral deconvolution thus shows that the extent of the decrease in B^{III} fraction is most pronounced for the B^{III} ring sites with only limited change in B^{IV} unlike previous findings [29, 46]. On the contrary, pressure-quenched B_2O_3 glass shows a decrease in fraction of non-ring structures with subsequent increase in fractions of both B^{III} ring and B^{IV} units [74].

Next, we consider the ^{27}Al and ^{31}P MAS NMR spectra in Figure 5c and Figure S4 in the Supplemental Material [45], respectively. The spectra of the as-prepared glass are dominated by Al^{IV} and $P^{(4)}$ units, respectively, with minor fraction of higher coordinated Al species as shown in Table 1 and Figure S5 in Supplemental Material [45]. The observed isotropic chemical shifts of around 36, 5, and -20 ppm for Al^{IV}, Al^V, and Al^{VI}, respectively, agree well with those of Al-based glasses with P as next nearest neighbor [75]. In agreement with the ^{11}B and ^{27}Al NMR results, the ^{31}P spectra are characterized by a dominant peak around -36 ppm attributed to the formation of $AlPO_4$ and BPO_4 units [76, 77]. Both the ^{27}Al and ^{31}P MAS NMR spectra exhibit negligible pressure-induced changes, likely due to the absence of significant amount of non-bridging oxygen (NBO) in the modifier-free glass [29]. We note that changes in aluminum speciation have previously been observed in Al-containing glasses without NBOs [78], but such changes are not observed here, as confirmed by the identical isotropic projections of their ^{27}Al 3QMAS NMR spectra (Figure S5 in Supplemental Material [45]).

IV. DISCUSSION

The cracking behavior of glasses under high stresses, such as during indentation, is believed to depend largely on the fracture toughness and associated fracture energy, and the relative fraction of the two

deformation mechanisms: volume-conservative shear flow and permanent densification [17, 21, 54]. The former is a function of bond strength of the constituent cation-oxygen bonds present in the glass structure (Al-O, B-O, P-O, Si-O in the present case) along with the surface concentration of such bonds, while the latter has been suggested to depend on C_g [11, 79], i.e., on the free volume of the starting material, which in turn depends on the glass chemistry and formation history. Compaction of glass by sub-T_g annealing or hot compression has been reported to result in significant differences in the indentation behavior, including an increase in H_V and a significant decrease in CR, which previous studies have related to a corresponding increase in C_g [79]. Intuitively, there would be less potential for further densification during indentation after network compaction. Both experiments and molecular dynamic simulations have indicated an increase in the extent of pile-up of matter in the vicinity of the imprint (i.e., shear flow) after high pressure treatments [43, 80], and displaying a smaller V_R value [43]. However, the present modifier-free mixed network glass exhibits an interesting exception to this behavior upon hot compression, showing an increase in the CR. This suggests that the atomic-scale structure and fracture surface energy needs to be considered and not only the intrinsic free-volume.

In general, pressure-induced structural changes in oxide glasses include changes in the next nearest neighbor distributions and ring statistics [81, 82], number of NBOs [83, 84], coordination number of network-former cations [85], and network former/modifier-oxygen bond angle/distances [82, 83]. The present glass exhibits very small changes in coordination numbers upon hot compression, in agreement with other previously investigated glasses with few NBOs [78]. Molecular dynamics simulations have previously suggested that the increase in density resulting from hot compression mostly affects the medium-range order (e.g., by reducing inter-tetrahedral bond angles or ring sizes) [29]. Such changes come with a relatively low energy cost, allowing the glass to densify to a certain extent. We therefore suggest that the pressure-induced increase in CR is attributed to the combination of the following two mechanisms:

(1) Network structure rearrangement: The major change observed in the present glass structure is an increase in the fraction of B$^{\text{III}}$ non-ring structural units along with some bond angle variations. The

presence of significant amount of B^{III} non-ring structural units in the hot compressed glass enhances the ability of the atomic network to densify by providing additional means for energy dissipation by accommodating mechanical stress through some rearrangements in the short-range order structure. The non-ring oxygens have been reported to have greater degree of flexibility than the rigidly constrained boroxol rings [86], and the B-O-B non-ring bonds exhibit a greater range of bond angles in comparison to ring units [86]. In addition, these B^{III} non-ring structural units have been reported to mix randomly in the glass structure in comparison to their ring counterparts, which tend to aggregate, and form constrained micro domains in the structure, which limits the atomic flexibility at low temperature [87-89]. Consequently, the fewer boroxol rings enhances the angular flexibility, which facilitates densification and thus maintains a nearly constant V_R value upon densification at elevated temperature.

(2) Increase in fracture surface energy: Fracture toughness of glasses governs the propagation of cracks from flaws/voids and might increase with compression due to an increase in the fracture surface energy [91,92]. The plausible reason for this increase is the increase in the number of bond constraints per unit of volume that need to be deformed under stress upon densification [91]. This would eventually require the crack front to break more bonds per unit of area to propagate, inducing a higher fracture surface energy. In turn, this implies an increasingly higher resistance to crack propagation in densified glass under higher pressure. However, in previous studies, we have observed a pressure-induced decrease in *CR* for various oxide glasses [29], which is due to the change in the indentation deformation mechanism. That is, the deformation mechanism changes from a primarily densification-driven to one based predominantly on shear flow, as manifested by the decrease in V_R (absent in the present case), which in turn overrides the expected increase in fracture surface energy due to hot compression [11,12,13].

As such, although pressure typically results in an increase in the number of constraints (and a decrease in atomic mobility), in the present glass the application of pressure results in a decrease in network rigidity through formation of structural states (e.g., B^{III} non-ring) with higher flexibility than the preceding structural units (B^{III} ring). This leads to an insignificant change in the V_R upon compression (within the error range), which does not counteract the effect of an increased fracture energy on CR. As

such, the anomalous densification behavior could explain the observed increase in crack resistance. That is, the intrinsic flexibility of the otherwise forbidden structural states increases the stress absorption ability of the glass through atomic reorganization upon indentation by facilitating further densification, which in turn reduces the residual stress.

V. CONCLUSIONS

The present study challenges the general understanding about the role of hot compression and free volume in controlling the mechanical properties of glasses, highlighting the importance of surface fracture energy and structural configurations with stress dissipation ability for achieving crack-resistant glasses. Specifically, we have enabled access to a forbidden structural state in a modifier-free mixed network $4Al_2O_3$-$28B_2O_3$-$10P_2O_5$-$58SiO_2$ glass through hot compression treatment, which showed an unexpected increase in both crack resistance and hardness. The structural characterization showed the formation of non-ring B^{III} units, which appear to govern the increasing degree of densification contribution during indentation after pre-compression. Micro-Raman scattering experiments also showed that the as-prepared and pre-compressed glasses undergo different structural changes during sharp-contact mechanical loading. This study thus pushes the boundaries of structural design of glasses beyond the phase space accessible through composition and thermal history variation alone.

REFERENCES

[1]   R. O. Ritchie, Nat. Mater. **10**, 817 (2011).

[2]   H. S. Gupta, W. Wagermaier, G. A. Zickler, D. Raz-Ben Aroush, S. S. Funari, P. Roschger, H. D. Wagner, and P. Fratzl, Nano Letters **5**, 2108 (2005).

[3]   G.B Olson and M Cohen, *Dislocations in Solids North-Holland,* F. R. N Nabarro edn., Vol. 7, (1986).

[4]   R. Z. Wang, Z. Suo, A. G. Evans, N. Yao, and I. A. Aksay, J. Mater. Resr **16**, 2485 (2011).

[5]   R. D. Conner, W. L. Johnson, N. E. Paton, and W. D. Nix, J. Appl. Phys. **94**, 904 (2003).

[6]   Z. Zhang, H. Sheng, Z. Wang, B. Gludovatz, Z. Zhang, E. P. George, Q. Yu, S. X. Mao, and R. O. Ritchie, Nat. Comm. **8**, 14390 (2017).

[7]   A. G. Evans, J. Am. Cer. Soc. **73**, 187 (1990).

[8]   J. C. Mauro, A. Tandia, K. D. Vargheese, Y. Z. Mauro, and M. M. Smedskjaer, Chem. Mater. **28**, 4267 (2016).

[9]   L. Wondraczek, J. C. Mauro, J. Eckert, U. Kuhn, J. Horbach, J. Deubener, and T. Rouxel, Adv. Mater. **23**, 4578 (2011).

[10]   S. Deriano, T. Rouxel, M. LeFloch, and B. Beuneu, Phys. Chem. Glasses **45**, 37 (2004).

[11]   K. Januchta, R. E. Youngman, A. Goel, M. Bauchy, S. J. Rzoska, M. Bockowski, and M. M. Smedskjaer, J. Non-Cryst. Solids **460**, 54 (2017).

[12]   K. Januchta, R. E. Youngman, A. Goel, M. Bauchy, S. L. Logunov, S. J. Rzoska, M. Bockowski, L. R. Jensen, and M. M. Smedskjaer, Chem. Mater. **29**, 5865 (2017)

[13]   K. G. Aakermann, K. Januchta, J. A. Pedersen, M. N. Svenson, S. J. Rzoska, M. Bockowski, J. C. Mauro, M. Guerette, L. Huang, and M. M. Smedskjaer, J. Non-Cryst. Solids 426, **175** (2015).

[14]   B. Pahari, S. Iftekhar, A. Jaworski, K. Okhotnikov, K. Jansson, B. Stevensson, J. Grins, and M. Edén, J. Am. Cer. Soc. **95**, 2545 (2012)

[15]   M. M. Smedskjaer, J. C. Mauro, and Y. Z. Yue, Phys. Rev. Lett. **05**, 115503 (2010).

[16]   S. Kapoor, N. Lönnroth, R. E. Youngman, S. J. Rzoska, M. Bockowski, L. R. Jensen, and M. M. Smedskjaer, J. Non-Cryst. Solids **469**, 31 (2017).

[17]   J. Luo, P. J. Lezzi, K. D. Vargheese, A. Tandia, J. T. Harris, T. M. Gross, and J. C. Mauro, Front. Mater. **3** (2016).

[18]   S. Karlsson, B. Jonson, and C. Stålhandske, Glass Technol. Eur. Glass Sci. Technol. A **51**, 41 (2010).

[19]   D. W. Rinehart, Chemical Strengthening of Glass, US 4119760, (October 10, 1978).

[20]   S. Louis, Method of thermal tempering transparent glass bodies, US 3620706, (Novermber 16, 1971).

[21]   T. Rouxel,. Phil. Trans. R. Soc. A **373**, 20140140 (2015).

[22]   B. Stevensson and M. Edén, J. Non-Cryst. Solids **378**, 163 (2013).

[23]   A. Rosenflanz, M. Frey, B. Endres, T. Anderson, E. Richards, and C. Schardt, Nature **430**, 761 (2004).

[24]   J. Johnson, R. Weber, and M. Grimsditch, J. Non-Cryst. Solids **351**, 650 (2005).

[25]   M. M. Smedskjaer, M. Bauchy, J. C. Mauro, S. J. Rzoska, and M. Bockowski, J. Chem. Phys. **143**, 164505 (2015).

[26]   G. L. Paraschiv, S. Gomez, J. C. Mauro, L. Wondraczek, Y. Yue and M. M. Smedskjaer, J. Phys. Chem. B **119,** 4109 (2015).

[27]   A. K.Varshneya, Int. J. Appl. Glass Sci. **1**, 131 (2010).

[28]   À. R. Garcia, C. Clausell, and A. Barba, Bol. Soc. Esp. Ceram. **55**, 209 (2016).

[29]   S. Kapoor, L. Wondraczek, and M. M. Smedskjaer, Front. Mater. **4** (2017).

[30]   M. N. Svenson, J. C. Mauro, S. J. Rzoska, M. Bockowski, and M. M. Smedskjaer, Sci. Rep. **7**, 46631 (2017).

[31]   S. Striepe, M. Potuzak, M. M. Smedskjaer, and J. Deubener, J. Non-Cryst. Solids **362**, 40 (2013).

[32]   K. Januchta, M Bauchy, R. E. Youngman, S. J. Rzoska, M. Bockowski, and M. M. Smedskjaer Phys. Rev. Mater. **1**, 063603 (2017).

[33]   G. A. Rosales-Sosa, A. Masuno, Y. Higo, H. Inoue, Y. Yanaba, T. Mizoguchi, T. Umada, K. Okamura, K. Kato, and Y. Watanabe, Sci. Rep. **5**, 15233 (2015).

[34]   A. Perriot, D. Vandembroucq, E. Barthel, V. Martinez, L. Grosvalet, C. Martinet, and B. Champagnon, J. Am. Cer. Soc. **89**, 596 (2006).

[35]   A. J. Ellison, J. C. Mauro, and N. Venkataraman, US20140335331 A1, (13 November, 2014).

[36]   A. Wolfenden, Dynamic elastic modulus measurements in materials ASTM International: 1990.

[37]   J. P. Amoureux, C Fernandez, and S Steuernagel, J. Mag. Res., **123**, 116 (1996).

[38]   D. Massiot, F. Fayon, M. Capron, I. King, S. L. Calv, B. Alonso, J. O. Durand, B. Bujoli, Z. Gan, and G. Hoatson, Magn. Reson. Chem. **40**, 70 (2002).

[39]   D. R. Neuville, L. Cormier, and D. Massiot, Geochim. Cosmochim. Acta 2004, 68, 5071.

[40]   D. R. Uhlmann, J. Non-Cryst. Solids **13**, 89 (1996).

[41]   K. Hirao, Z Zhang, H Morta, and N Soga, J. Soc. Mater. Sci. Jpn. **40**, 400 (1991).

[42]   M. N. Svenson, T. K. Bechgaard, S. D. Fuglsang, R. H. Pedersen, A. Ø. Tjell, M. B. Østergaard, R. E. Youngman, J. C. Mauro, S. J. Rzoska, M. Bockowski, and M. M. Smedskjaer, Phy. Rev. Appl. **2**, 024006 (1991).

[43]   T. Rouxel, H. Ji, J. Guin, F. Augereau, and B. Rufflé, J. Appl. Phy. **107**, 094903 (1991).

[44]   R.T. Shannon, Acta Crystallogr., Sect. A: Cryst. Phys., Diffr., Theor. Gen. Crystallogr. **32**, 751 (1976).

[45]   See Supplemental Material for further details about density dependence of elastic moduli, ^{31}P MAS NMR spectra, ^{11}B and ^{27}Al 3QMAS NMR spectra, and summary of physical property data

[46]   S. Kapoor, X. Guo, R. E. Youngman, C. L. Hogue, J. C. Mauro, S. J. Rzoska, M. Bockowski, L. R. Jensen, and M. M. Smedskjaer, Phys. Rev. Appl. **7**, 054011 (2017).

[47]   K. Hirao, M. Yoshimoto, N. Soga, and K. Tanaka, J. Non-Cryst. Solids **130**, 78 (1991).

[48]   Z. Y. Yao, D. Möncke, E. I. Kamitsos, P. Houizot, F. Célarié, T. Rouxel, and L. Wondraczek, J. Non-Cryst. Solids **435**, 55 (2016).

[49]   M. N. Svenson, M. Guerette, L. Huang, N. Lonnroth, J. C. Mauro, S. J. Rzoska, M. Bockowski, and M. M. Smedskjaer, Chem. Phys. Lett. **651**, 88 (2016).

[50]   B. R. Lawn and V. R. Howes, J. Mater. Sci. **16**, 2745 (1981).

[51]   M. Bauchy, B. Wang, M. Wang, Y. Yu, M. J. Abdolhosseini Qomi, M. M. Smedskjaer, C. Bichara, F. J. Ulm, and R. Pellenq, Acta Mater. **121**, 234 (2016).

[52]   Y. Kato, H. Yamazaki, S. Yoshida, and J. Matsuoka, J. Non-Cryst. Solids **356**, 1768 (2010).

[53]   K. Yoshinari, H. Yamazaki, S. Itakura, S. Yoshida, and J. Matsuoka, J. Cer. Soc. Jpn. **119**, 110 (2011).

[54]   S. Yoshida, J. C. Sangleboeuf, and T. Rouxel, J. Mater. Res. **20**, 3404 (2005).

[55]   C. L. Losq, D. R. Neuville, P. Florian, G. S. Henderson, and D. Massiot. Geochim. Cosmochim. Acta **126**, 495 (2014).

[56]   M. Guerette, M. R. Ackerson, J. Thomas, F. Yuan, E. B. Watson, D. Walker, and L. Huang, Sci. Rep. **5**, 15343 (2015).

[57]   B. T. Poe, C. Romano, and G. Henderson, J. Non-Cryst. Solids **341**, 162 (2004).

[58]   W. L. Konijnendijk and J. M. Stevels, J. Non-Cryst. Solids, **18**, 307 (1975).

[59]   T. Uesbeck, H. Eckert, R. Youngman, and B. Aitken, J. Phys. Chem. C **121**, 1838 (2017).

[60]   M. Grimsditch, A. Polian, and A. C. Wright, Phys. Rev. B **54**, 152 (1996).

[61]   A. C. Wright, C. E. Stone, R. N. Sinclair, N. Umesaki, N. Kitamura, K. Ura, N. Ohtori, and A. C. Hannon, Phys. Chem. Glasses **41**, 296 (2000).

[62]   J. E. Dickinson Jr, and B. W. H. S. Jong J. Non-Cryst. Solids **102**, 196 (1988).

[63]   B. O. Mysen, F. Holtz, M. Pichavant, J. M. Beny, and J. M. Montel, Am. Miner. **84**, 1336 (1999).

[64]   P. H. Larsen, F. W. Poulsen, and R. W. Berg, J. Non-Cryst. Solids **244**, 16 (1999).

[65]   F. L. Galeener, Solid State Comm. **44**, 1037 (1982).

[66]   A. Winterstein-Beckmann, D. Moncke, D. Palles, E. I. Kamitsos, and L. Wondraczek, J. Non-Cryst. Solids **401**, 110 (2014).

[67]   T. Furukawa, K. E. Fox, and W. B. White, J. Chem. Phys. **75**, 3226 (1981).

[68]   A. K. Yadav and P. Singh, RSC Adv. **5**, 67583 (2015).

[69]   M. N. Svenson, M. Guerette, L. Huang, and M. M. Smedskjaer, J. Non-Cryst. Solids **443**, 130 (2016).

[70]   B. N. Meera and J. Ramakrishna, J. Non-Cryst. Solids **159**, 1 (1993).

[71]   M. N. Svenson, R. E. Youngman, Y. Yue, S. J. Rzoska, M. Bockowski, L. R. Jensen, and M. M. Smedskjaer, Phys. Chem. Chem. Phys. **18** , 29879 (2016).

[72]   A. R. Grimmer, D. Müller, G. Gözel, and R. Kniep, Fresenius J. Anal. Chem. **357**, 485 (1997).

[73]   M. B. Ostergaard, R. E. Youngman, M. N. Svenson, S. J. Rzoska, M. Bockowski, L. R. Jensen, and M. M. Smedskjaer, RSC Adv. **5**, 78845 (2015).

[74]   S. K. Lee, K. Mibe, Y. Fei, G. D. Cody, and B. O. Mysen, Phys. Rev. Lett. **94**, 165507 (2005).

[75]   K. J. MacKenzie and M. E. Smith, *Multinuclear solid-state nuclear magnetic resonance of inorganic materials*, Elsevier, 2002.

[76]   A. W. Buckermann, C. Mundus, and W. Miiller-Warmuth, J. Non-Cryst. Solids **208**, 217 (1996).

[77]   G. L. Turner, K. A. Smith, R. J. Kirkpatrick, and E. Oldfieldt, J. Mag. Reson. (1969) **70**, 408 (1986).

[78]   J. R. Allwardt, B. T. Poe, and J. F. Stebbins, Am Miner. **90**, 1453 (2005).

[79]   Z. Zhang, N. Soga, and K. Hirao, J. Mater. Sci. **30**, 6359 (1995).

[80]   F. Yuan and L. Huang, Sci. Rep. **4**, 5035 (2014).

[81]   S. K. Lee, Solid State Nucl. Magn. Reson. **38**, 45 (2010).

[82]   C. Sonneville, D. De Ligny, A. Mermet, B. Champagnon, C. Martinet, G. Henderson, T. Deschamps, J. Margueritat and E. Barthel, J. Chem. Phys. **139**, 074501 (2013).

[83]   X. Xue and J. F. Stebbins, Phys. Chem. Miner. **20**, 297 (1993).

[84]   A. George and J. Stebbins, Phys Chem. Miner. **23**, 526 (1996).

[85]   M. M. Smedskjaer, R. E. Youngman, S. Striepe, M. Potuzak, U. Bauer, J. Deubener, H. Behrens, J. C. Mauro, and Y. Yue. Sci. Rep. **4** (2014).

[86]   A. Wong, A. P. Howes, B. Parkinson, T. Anupold, A. Samoson, D. Holland, and R. Dupree, Phys. Chem. Chem. Phys. **11**, 7061 (2009).

[87]   E. M. Pierce, L. R. Reed, W. J. Shaw, B. P. McGrail, J. P. Icenhower, C. F. Windisch, E. A. Cordova, and J. Broady, Geochim. Cosmochim. Acta **74**, 2634 (2010).

[88]   L. S. Du and J. F. Stebbins. Solid State Nuc. Mag. Reson. **27**, 37 (2005).

[89]   L. S. Du and J. F. Stebbins, J. Non-Cryst. Solids **315**, 239 (2003).

[90]   T. K. Bechgaard, A. Goel, R. E. Youngman, J. C. Mauro, S. J. Rzoska, M. Bockowski, L. R. Jensen, and M. M. Smedskjaer, J. Non-Cryst. Solids **441**, 49 (2016).

[91]   F. Yuan and L. Huang, Sci. Rep. **4**, 5035 (2014).

[92]   T Rouxel, Scripta Materialia **137**, 109-113 (2017)

TABLE I. Boron and aluminum speciation derived from ^{11}B and ^{27}Al MAS NMR measurements on the as-prepared and hot compressed samples. Uncertainties in the boron and aluminum speciation are approximately ±1% and ±2%, respectively.

Glass	B^{III} [%]				$[B^{III}_{ring}]/$ $[B^{III}_{non-ring}]$	B^{IV} [%]	Al^{IV} [%]	Al^{V} [%]	Al^{VI} [%]
	Ring	C_Q (MHz)	Non-ring	C_Q (MHz)					
As-prepared	16.0	2.71	63.4	2.64	0.25	20.6	79.7	16.5	3.9
Hot compressed	10.3	2.75	69.3	2.65	0.15	20.4	80.0	16.9	3.1
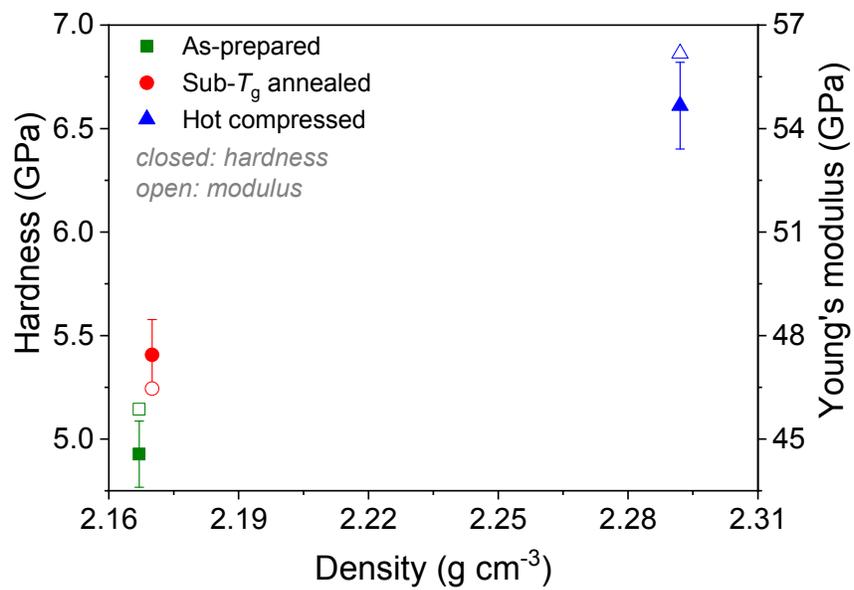
FIG 1. Density dependence of Vicker's hardness (closed symbols) at 0.05 kgf and Young's modulus (open symbols, determined using pulse-echo method) for three samples: as-prepared, annealed at $0.9T_g$, and 1 GPa compressed at T_g. The error in Young's modulus is within ± 1 GPa.
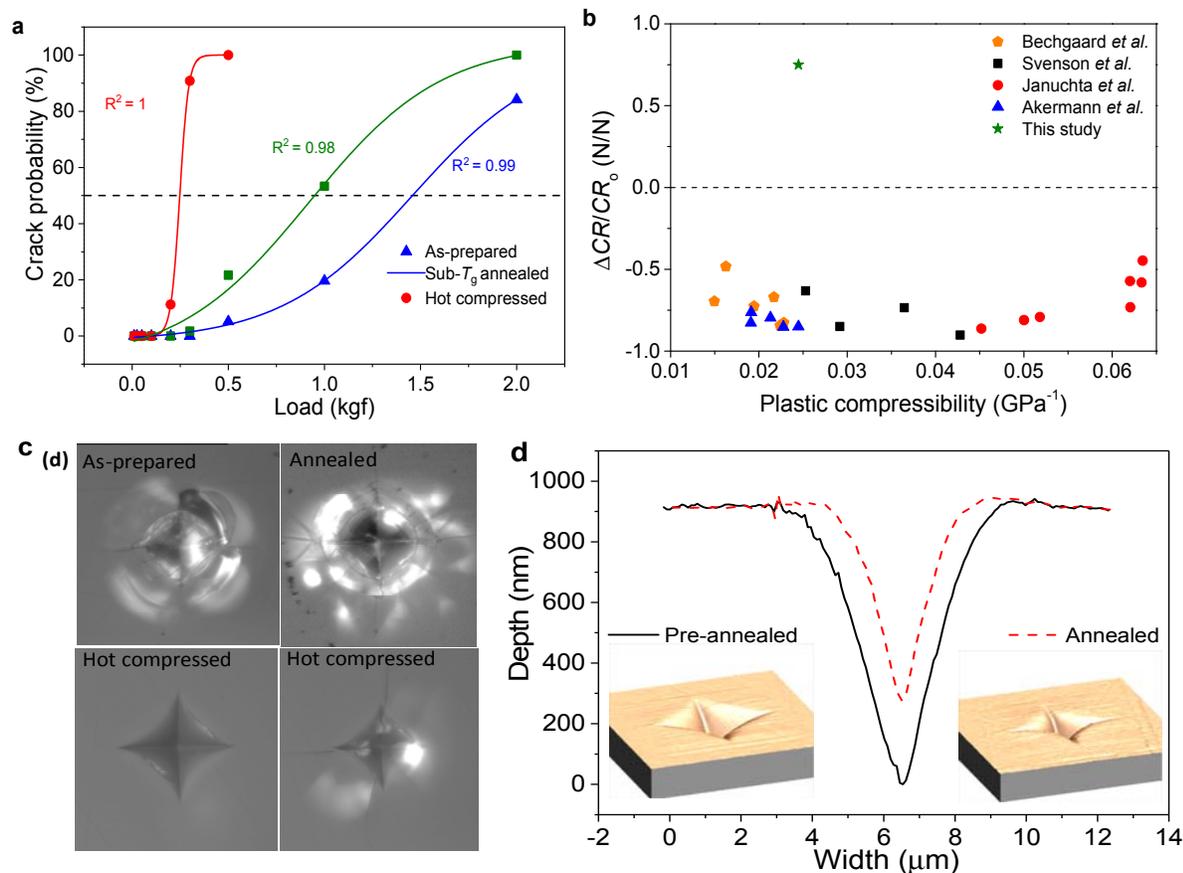
FIG 2. Cracking behavior of as-prepared and densified glass. **(a)** Crack probability as a function of applied indentation load for the as-prepared, annealed ($0.9T_g$ for 16 h), and hot compressed (1 GPa at T_g) modifier-free glass. **(b)** Change in crack resistance CR upon hot compression ($\Delta CR/CR_o$), including present and literature data [12, 13, 42, 90], as a function of plastic compressibility, which quantifies the extent of permanent densification upon compression ($-(1/V)(dV/dp)$). Lines are intended as guides for the eye. **(c)** Optical images of indents produced at 1 kgf on the surface of the as-prepared, sub-T_g annealed, hot compressed (without cracks), and hot compressed (with two cracks) samples, respectively. **(d)** Topography of an indent produced at 25 gf in the as-prepared glass shown as cross-sections before and after annealing at $0.9T_g$ for 2 h. The respective 3D-images are also shown.
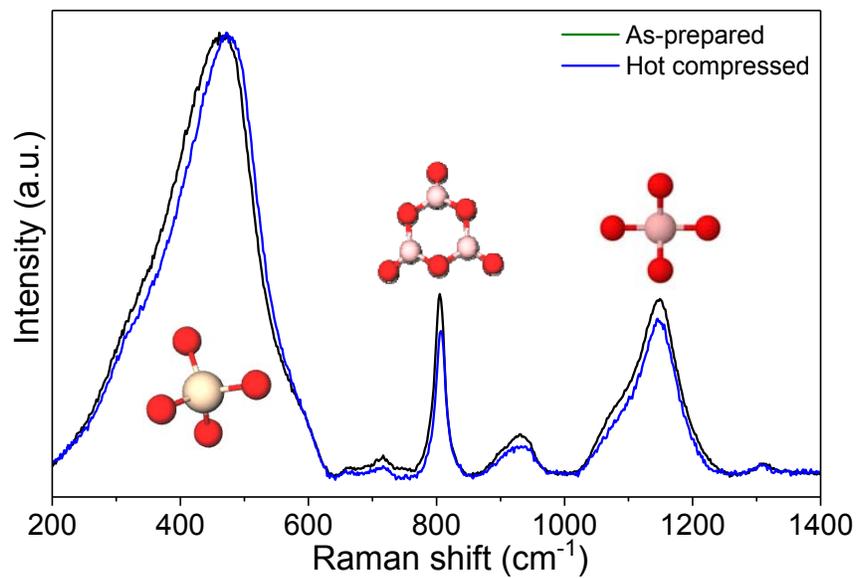
FIG 3. Structural changes following hot compression. Raman spectra of the as-prepared (black) and hot compressed glass (blue). The structural units associated with the three main bands are illustrated.
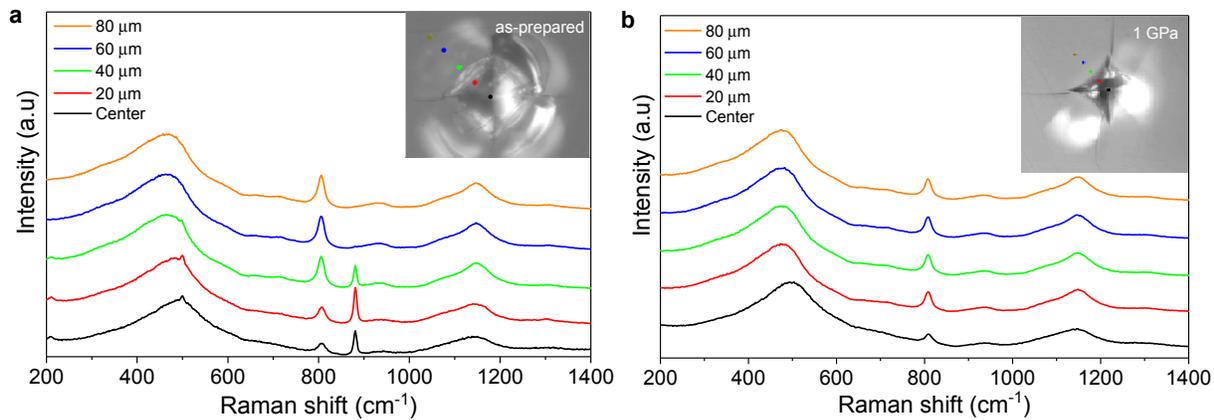
FIG 4. Micro-Raman spectroscopy analysis of indented glasses. Spectra of **(a)** as-prepared and **(b)** hot compressed glass recorded at increasing distances from the center of an indent produced at 1 kgf. Insets show the top view of these indents with the marked positions of laser focus.
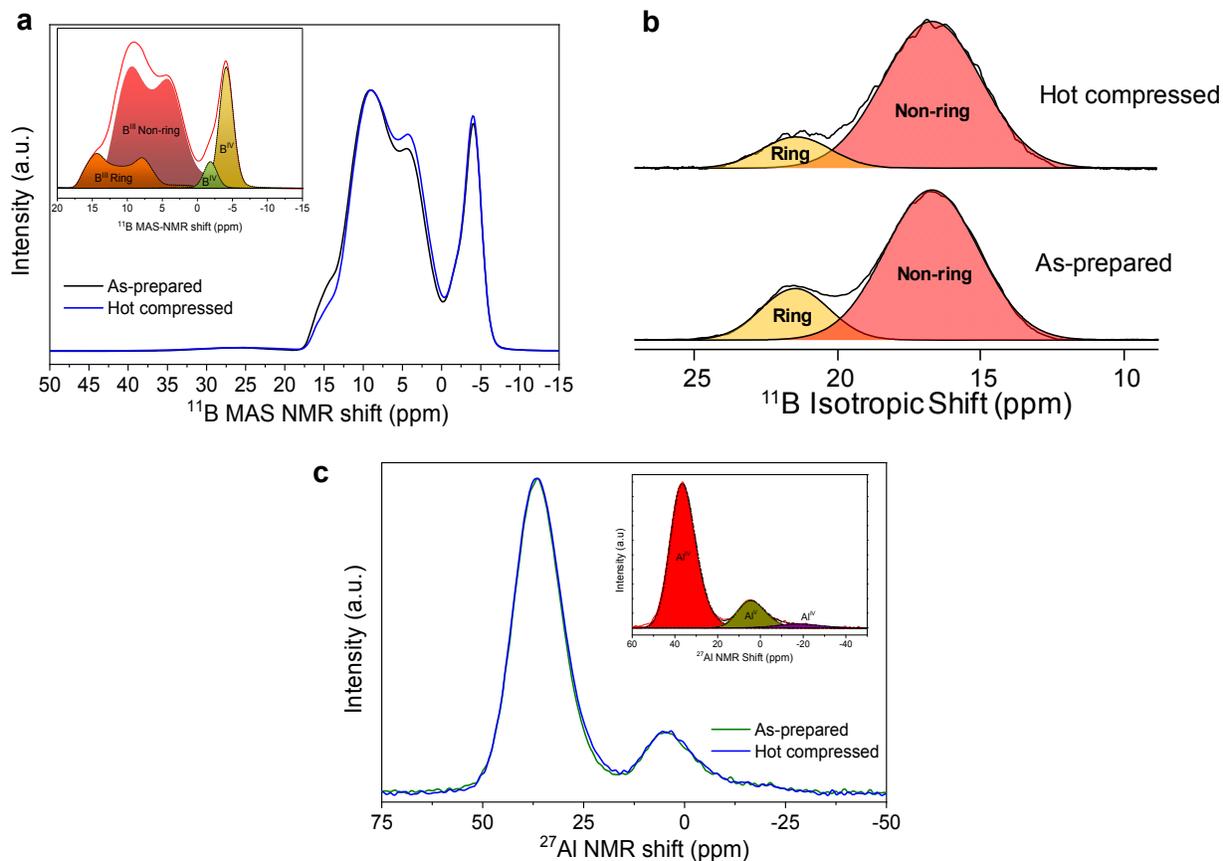
FIG 5. Solid state NMR spectroscopy analysis of as-prepared and hot compressed glass. (**a**) ^{11}B MAS NMR spectra for the as-prepared and hot compressed glasses obtained at 11.7 T. Inset: deconvoluted spectrum of as-prepared glass. (**b**) Isotropic projections of ^{11}B 3QMAS NMR spectra for the as-prepared and hot compressed glass. (**c**) ^{27}Al MAS NMR spectra for the as-prepared and hot compressed glass. Inset: deconvoluted spectrum of as-prepared glass

GRAPHICAL ABSTRACT